Review

Effects of Electron Backscattering in Auger Electron Spectroscopy: Recent Developments

A. Jablonski[a,*] and C. J. Powell[b]

[a]Institute of Physical Chemistry, Polish Academy of Sciences, ul. Kasprzaka 44/52, 01-224 Warsaw, Poland
[b]Surface and Microanalysis Science Division, National Institute of Standards and Technology,
Gaithersburg, Maryland 20899-8370, USA
[*]jablo@ichf.edu.pl

There is currently increasing interest in a more complete theoretical description of the signal intensity in Auger electron spectroscopy (AES). We report calculations of backscattering factors (BFs) for three selected Auger transitions (Al $KL_{23}L_{23}$, Pd $M_5N_{45}N_{45}$, and Pt $M_5N_{67}N_{67}$) in the corresponding elemental solids using two algorithms. With algorithm A, BF values were obtained with a Monte Carlo calculation in which individual inelastic-scattering events were simulated. With the more approximate, but faster algorithm B, BFs were calculated using the continuous slowing-down approximation and stopping powers from a recently developed predictive formula. For primary-beam energies between 3 keV and 20 keV, differences in BFs from the two algorithms ranged between 1.3 % and 9 % for the three Auger transitions. These differences arose mainly from limitations of the predictive formula for the stopping power with algorithm B. Nevertheless, the differences are believed to be sufficiently small to enable use of the faster algorithm B for many applications in quantitative AES.

1. Introduction

In Auger-electron spectroscopy (AES) of solid surfaces, part of the measured signal is due to Auger electrons resulting from the decay of inner-shell vacancies created by the primary beam while another part of the signal is due to Auger electrons from similar vacancies created by backscattered electrons (i.e., primary electrons that have been inelastically backscattered to the surface region responsible for the detected signal). Consequently, the degree to which the signal is enhanced must be accounted for in quantitative applications of AES. By convention, secondary electrons with energies larger than 50 eV are termed backscattered electrons although only those electrons with energies larger than the threshold for inner-shell ionization in a particular sample need to be considered in BF determinations.

The backscattering problem was recognized in 1969 by Bishop and Riviere [1] who proposed the term backscattering factor (BF) to describe the Auger-signal enhancement due to backscattered electrons. These authors also calculated the first BF values for selected elemental solids. Goto and coworkers [2,3] proposed an interesting experimental method in the 1970s for determining the BF. This method consisted of consecutive depositions of a low-atomic-number element (beryllium) onto a medium-atomic-number substrate (copper). After each increment of Be deposition, measurements were made of the Be Auger intensity and the backscattering coefficient, η, the probability of backscattering for electrons with energies exceeding 50 eV. The principle of the method is illustrated in Fig. 1 where the arrows indicate results for increasing Be thickness. The experimental curve for thick Be films was then extrapolated to the η=0 axis. It was assumed that the extrapolated Auger-signal intensity, I_{ext}, results only from inner-shell ionizations from the primary beam. The backscattering factor, r, for Be was then obtained from the simple relation,

$$r = I_{Be}/I_{ext} , \qquad (1)$$

where I_{Be} is the Be Auger intensity for the thickest Be film (Fig. 1). Other methods for determining BFs are

Journal of Surface Analysis Vol.15, No. 2 (2008) pp. 139−149

A. Jablonski et al.   Effects of Electron Backscattering in Auger Electron Spectroscopy: Recent Developments

described in a 1979 review by Jablonski [4] who also discussed theoretical methods for obtaining BFs.
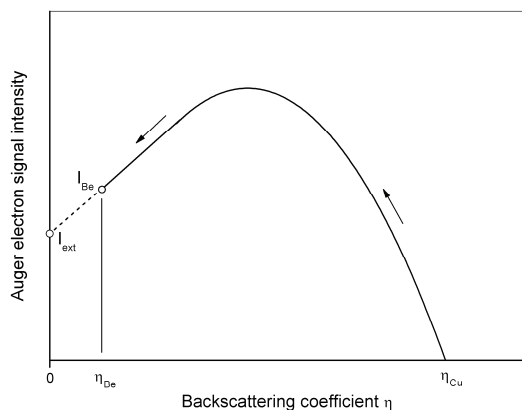

Fig. 1. Principle of the Goto method for determination of the backscattering factor [2,3]. In these experiments, the Be Auger-electron signal intensity was plotted as a function of the backscattering coefficient as successive layers of Be were deposited on a Cu substrate. The arrows indicate increasing Be deposition, during which the backscattering coefficient changed from the value for bulk Cu, η_{Cu}, to the value for bulk Be, η_{Be} (see text).

An extensive database of BFs from Monte Carlo simulations for 25 materials with a wide range of atomic numbers was published by Shimizu and Ichimura [5-8] over 25 years ago for primary energies of 3 keV, 5 keV, 7.5 keV, and 10 keV and angles of primary-beam incidence of 0°, 30°, and 45° with respect to the surface normal. The BF data were fitted by simple analytical expressions [8] that are convenient and still generally used in current calculations for quantitative AES analyses. While the Shimizu and Ichimura simulations were performed for AES instrumental conditions in use at the time, modern AES instruments are operated with primary energies up to 25 keV. It is thus necessary to extrapolate the Shimizu expressions to much higher energies than those used in the original simulations.

Jablonski [9] has shown that the definition typically used in both theoretical and experimental methods for determination of the BF is oversimplified. Some of the assumptions made in describing the Auger-signal intensity are less valid in certain experimental configurations (e.g., grazing incidence of the primary beam) or for certain primary energies (e.g., close to the threshold for in-

ner-shell ionization for a particular sample). In such cases, we may expect significant systematic errors. A general definition has been proposed which transforms to the commonly used definition for typical simplifying assumptions. Different algorithms for calculating the BF from the general definition have been proposed [9-12]. It has been shown that, in certain analytical situations, BFs from the general definition can differ appreciably from values obtained from the simplified expression.

A more extensive set of BFs is now needed for quantitative AES with modern Auger instruments (i.e., for any solid and for common measurement conditions). Efficient calculations of the BF from the general definition are feasible with use of the continuous slowing-down approximation (CSDA) for describing inelastic scattering in the sample [12]. If a predictive formula is available for the electron stopping power (SP), we have all the tools to develop a universal algorithm that provides BF values for any sample. This topic is the subject of the present review.

2. Definition of the backscattering factor

According to terminology standards [13,14], the BF is defined as the fractional increase in the Auger current due to backscattered electrons. The BF is typically expressed by the formula,

$$r = 1 + \frac{\cos\theta_0}{I_0 \sigma_i(E_0)} \int_{E_c}^{E_0} \int_0^{\pi/2} I_B(E,\alpha)\, \sigma_i(E)\, \sec\alpha\, d\alpha\, dE, \quad (2)$$

where θ_0 is the incidence angle of the primary-electron beam, $\sigma_i(E_0)$ is the relevant inner-shell ionization cross section at the primary energy E_0, I_0 is the primary current, E_c is the threshold energy for inner-shell ionization, and $I_B(E,\alpha)$ is the current of backscattered electrons emitted from the sample with energy E and at an angle α with respect to the surface normal. Equation (2) is not convenient for practical calculations since the integrand approaches infinity at glancing emission angles. It is frequently assumed that the distribution of emission angles for the backscattered electrons, $g(\alpha)$, is independent of their energy:

$$I_B(E,\alpha) = I_B(E)\, g(\alpha). \quad (3)$$

Consequently, we obtain the simple expression,

Journal of Surface Analysis Vol.15, No. 2 (2008) pp. 139−149

A. Jablonski et al.   Effects of Electron Backscattering in Auger Electron Spectroscopy: Recent Developments

$$r = 1 + \frac{<\sec\alpha>}{I_0 \sigma_i(E_0)\sec\theta_0} \int_{E_c}^{E_0} I_B(E)\sigma_i(E)dE, \qquad (4)$$

where $<\sec\alpha>$ is the mean value of the secant of emission angles. For an AES configuration with normal incidence of the primary beam, it is reasonable to assume that the emission angles of backscattered electrons follow a cosine distribution, and thus $g(\alpha)=2\sin\alpha\cos\alpha$. The value of $<\sec\alpha>$ is then 2, and

$$r = 1 + \frac{2}{I_0\sigma_i(E_0)} \int_{E_c}^{E_0} I_B(E)\,\sigma_i(E)\,dE. \qquad (5)$$

The Monte Carlo simulations of Shimizu and Ichimura [5-7] were based on Eq. (4). Shimizu [8] performed least-squares fits of the BFs from these simulations to three simple analytical formulas,

$$r = 1 + (2.34 - 2.10Z^{0.14})\,U_0^{-0.35}$$
$$+ (2.58Z^{0.14} - 2.98) \qquad (\text{for } \theta_0 = 0°) \qquad (6a)$$

$$r = 1 + (0.462 - 0.777Z^{0.20})\,U_0^{-0.32}$$
$$+ (1.15Z^{0.20} - 1.05) \qquad (\text{for } \theta_0 = 30°) \qquad (6b)$$

$$r = 1 + (1.21 - 1.39Z^{0.13})\,U_0^{-0.33}$$
$$+ (1.94Z^{0.13} - 1.88) \qquad (\text{for } \theta_0 = 45°) \qquad (6c)$$

where Z is the atomic number, and U_0 is the ratio E_0/E_c. These fits were valid for primary energies between $E_0 = 3\ 000$ eV and $E_0 = 10\ 000$ eV. We see that BFs from Eqs. (6) are a function of the atomic number, Z, the primary energy, E_0, the threshold energy for inner-shell ionization, E_c, and the primary-beam incidence angle, θ_0. Due to their simplicity and convenience, the Shimizu expressions are widely used in quantitative Auger analyses. For application of Eqs. (6) to compounds, an average atomic number is introduced, although a compound containing low and high atomic-number elements tends to have a larger BF than an elemental solid with the corresponding average atomic number [8].

The following assumptions were made in the derivation of the expression defining the BF [Eq. (2)]:

1. The primary beam passes through the near-surface region of the sample from which most of the detected Auger signal originates without significant attenuation of the primary-beam current or reduction of the primary-beam energy. We note here that the information depth for the detected signal can be evaluated as de-

scribed elsewhere [15].

2. The angular and energy distribution of electrons back-scattered from the sample $[I_B(E,\alpha)]$ is identical to this distribution in the near-surface region.

3. Inner-shell ionizations by backscattered electrons traveling into the solid in the near-surface region are ignored.

A further assumption in the derivation of Eqs. (4) and (5) is that the energy and angular distributions of backscattered electrons are independent of each other. These assumptions may lead to systematic errors in BF values obtained from Eq. (5). To avoid these errors, a general definition of the BF was proposed in which these assumptions are not made [9]. The BF is then defined as an integral over depth, z, of the product of the excitation depth distribution function (EXDDF), $\Phi(z,E_0,\theta_0)$, and the emission depth distribution function (EMDDF), $\phi(z,E_A,\alpha)$:

$$r = \int_0^\infty \Phi(z,E_c,E_0,\theta_0)\,\phi(\alpha,E_A,z)\,dz, \qquad (7)$$

where E_A is the Auger-electron energy. The EXDDF is defined as the probability that specified excitations are created at specified depths measured normally from a surface into the material by a beam of specified particles or radiation incident on the surface in a given direction [13,14]. The EMDDF is defined as the probability that the particle or radiation leaving the surface in a specified state in a given direction, originated from a specified depth measured normally from the surface into the material [13,14]. It is of crucial importance to normalize both functions properly in calculations of the BF from Eq. (7). The EXDDF must be normalized with respect to an isolated thin layer of the solid (in the same way as the "Phi-Rho-Z" function of electron microprobe analysis (EPMA) is normalized). The latter function is the ratio of the number of inner-shell ionizations in a thin layer at depth z in the solid to the number of similar ionizations in an isolated layer of the same thickness. The EMDDF is normalized so that the integral over this function with respect to depth is equal to unity.

3. Theoretical models for BF calculations

Different theoretical models have been implemented in calculations of the BF from Eq. (7) since both functions, the EXDDF and the EMDDF, can be determined from

Journal of Surface Analysis Vol.15, No. 2 (2008) pp. 139−149

A. Jablonski et al.   Effects of Electron Backscattering in Auger Electron Spectroscopy: Recent Developments

different algorithms. The EMDDF can be calculated from one of the analytical expressions derived from electron-transport theory [16-19]. In fact, the expression derived by Tilinin *et al.* [17] was used in the first BF calculations based on the general definition of the BF [9]. In a separate analysis, this expression was shown to be the most reliable analytical representation of the EMDDF [20]. The EMDDF can also be calculated from Monte Carlo simulations of Auger-electron trajectories [20]. This approach is considered to be the most accurate since it is based on a realistic theoretical model of electron transport. The Monte Carlo approach for calculating the EMDDF has been used in the majority of algorithms for calculating BFs from the general definition [10-12].

Calculation of the EXDDF, however, is a major theoretical challenge. Due to the complexity of the problem, it is appropriate to use the Monte Carlo method to simulate primary-electron trajectories in the solid with separate elastic and inelastic interactions along an electron trajectory. It is assumed that both interactions can be described by independent Poisson stochastic processes. To simulate the inelastic interactions, we need to know the differential inverse inelastic mean free path (DIIMFP). This function, denoted by $K(E,T)$ describes the distribution of energy losses, T, at an electron energy E. The probability density function of energy losses, $H(T|E)$, to be simulated in the Monte Carlo code, has a simple form,

$$H(T \mid E) = \frac{K(E,T)}{\int_0^E K(E,T)\, dT} . \qquad (8)$$

For computational convenience, we may assume that the DIIMFP is proportional to the energy-loss function in the optical limit, i.e., for the momentum transfer, q, approaching zero,

$$K(E,T) \propto \lim_{q \to 0} \text{Im}\left[-\frac{1}{\varepsilon(\omega,q)}\right], \qquad (9)$$

where $\varepsilon(\omega,q)$ is the complex dielectric constant which is a function of frequency ω (related to the energy loss by $T=\hbar\omega$) and q. This assumption was made in the BF calculations reported by Jablonski and Powell [10,12]. For rough guidance, one could use the "universal cross section" of Tougaard [21] to describe the distribution of energy losses,

$$K(E,T) = \frac{1}{\lambda_{in}} \frac{BT}{(C + T^2)^2} \qquad (10),$$

where λ_{in} is the electron inelastic mean free path (IMFP), and B and C are constant coefficients equal to 2866 eV^2 and 1643 eV^2, respectively. While Eq. (10) has been utilized in calculations of the EXDDF [9,22], one can expect considerable systematic errors for two reasons. First, the "universal cross section" was derived to describe relatively small energy losses, not exceeding 50 eV. Second, the "universal cross section" deviates considerably from the DIIMFP for some elements (e.g., silicon). Tougaard, however, has proposed alternative expressions to Eq. (10) for separate classes of materials [23].

Calculations of the EXDDF using Eqs. (8) and (9) can be performed only for a limited number of materials for which the energy-loss function is known. Nevertheless, it has been shown that a Monte Carlo strategy implementing the continuous slowing-down approximation (CSDA) provides accurate BF values at sufficiently high primary-electron energies while being much faster than conventional simulations in which individual inelastic interactions are modeled [24]. Preliminary results [24] indicate that the lower primary-energy limit is about 1000 eV, which is much lower than the primary energies typically used in AES. These tests were based on CSDA simulations with stopping powers derived from the same source as used to describe the energy-loss function.

EXDDF calculations based on the CSDA require knowledge of the stopping power (SP) for a given sample. The latter parameter, defined as the electron energy change per unit distance along the electron trajectory, is available from several sources, as discussed by Jablonski *et al.* [24]. Jablonski and Powell [12] have shown that the CSDA approach for determining EXDDFs will enable BF calculations to be made for any solid provided the needed SPs are available. This universal approach is, of course, very attractive.

Stopping-power data for electron energies less than about 30 keV are available only for a limited number of solids [25,26]. In addition, the well-known Bethe stopping-power equation is known to be valid only for electron energies larger than about 10 keV [25,26]. An attempt has therefore been made to derive a predictive SP equation [27,28]. It was found that the product of the

Journal of Surface Analysis Vol.15, No. 2 (2008) pp. 139−149

A. Jablonski et al.   Effects of Electron Backscattering in Auger Electron Spectroscopy: Recent Developments

stopping power, S, and the IMFP is a relatively weak function of electron energy, E, and atomic number, Z. A simple expression providing predicted values of the stopping power, S_{pred}, was derived from an analysis of SPs and IMFPs calculated from experimental optical data for 27 elemental solids [27,28],

$$S_{pred}\lambda_{in} = c_1(c_2 Z + 1)\ln(c_3 E) \qquad (11)$$

where S_{pred} is expressed in eV/Å, λ_{in} in Å, E in eV, and c_1 = 11.52 eV, c_2 = 0.01639, and c_3 = 0.03386 eV^{-1}. Equation (11) is valid for electron energies between 200 eV and 30 keV. The mean percentage deviation of the predicted SP values from the reference SP values obtained from optical data was 10.4 % [27,28]. We illustrate the quality of the fit for three selected elements (Al, Pd, and Pt) in Fig. 2. In the upper panels, we compare SPs calculated from optical data with values of S_{pred} from Eq. (11). The lower panels show the percentage deviation, ΔS, between the predicted and optical SPs,

$$\Delta S = 100 \frac{S_{opt} - S_{pred}}{S_{opt}}, \qquad (12)$$

where S_{opt} denotes SPs calculated from optical data. The solids chosen for Fig. 2 illustrate three cases: (i) a relatively poor fit, with deviations reaching 30 % (Fig. 2(a) for Al), (ii) a medium-quality fit (Fig. 2(b) for Pd), and (iii) a high-quality fit (Fig. 2(c) for Pt). As shown in a recent report [12], the differences between S_{opt} and S_{pred} influence the BF values obtained from Eq. (7). BF calculations for four illustrative solids based on Monte Carlo simulations of individual scattering events for the EXDDF and use of the CSDA with values of S_{pred} showed differences of < 2 % for Au, < 5 % for Ag, < 7 % for Cu, and < 10 % for Si for primary energies likely to be used in practical AES [12].

4. Results and Discussion

BF calculations were performed for three selected Auger transitions (Al $KL_{23}L_{23}$, Pd $M_5N_{45}N_{45}$, and Pt $M_5N_{67}N_{67}$) in the respective elemental solids using two algorithms. With algorithm A, reference BF values were obtained from Eq. (7) with a Monte Carlo calculation of the EXDDF in which individual inelastic-scattering events were simulated [10]. With algorithm B, BFs were calculated using Eq. (7) and the EXDDF was determined using the CSDA with predicted SPs from Eq. (11), as proposed by Jablonski and Powell [12]; an interested reader is referred to that paper for details. In both algorithms, a Monte Carlo simulation was made of elastic-scattering events, with differential elastic-scattering cross sections taken from the NIST Electron Elastic-Scattering Cross-Section Database [29]. The Casnati *et al.* [30] empirical formula for K-shell ionization cross sections was used in both calculations since this formula also adequately represents L-shell, M-shell, and N-shell ionization cross sections [31]. The thresholds for inner-shell ionization (binding energies), E_c and the Auger-electron energies, E_A, were taken from the NIST X-ray Photoelectron Spectroscopy database [32]. The IMFP values, calculated from optical data [33], were taken from the NIST Electron Inelastic-Mean-Free-Path Database [34]. Numerical values of the above parameters, used in calculations of the BF, are listed in Table 1.

As an illustration, consecutive stages of the BF calculations for the Pd $M_5N_{45}N_{45}$ Auger transition are shown in Fig. 3 for a selected set of measurement conditions (θ_0 = 0°, E_0 = 2 keV, and α = 10°). We first calculate the EMDDF, as shown in Fig. 3(a). Second, EXDDFs were calculated from algorithms A and B, as shown in Fig. 3(b). Third, the product of the EMDDF and EXDDF is calculated, as shown in Fig. 3(c), and then integrated to

Table 1. Values of parameters used in calculations of the backscattering factor.

Element	Auger transition	Auger-electron energy[a] (eV)	IMFP of Auger electrons[b] (Å)	Ionized level	Binding energy[a] (eV)
Al	$KL_{23}L_{23}$	1393	25.4	1s	1559
Pd	$M_5N_{45}N_{45}$	328	8.38	$3d_{5/2}$	335
Pt	$M_5N_{67}N_{67}$	1961	21.53	$3d_{5/2}$	2122

[a]Values from Ref. 32 (averaged values).
[b]Values from Refs 33 and 34.

Journal of Surface Analysis Vol.15, No. 2 (2008) pp. 139−149

A. Jablonski et al.   Effects of Electron Backscattering in Auger Electron Spectroscopy: Recent Developments
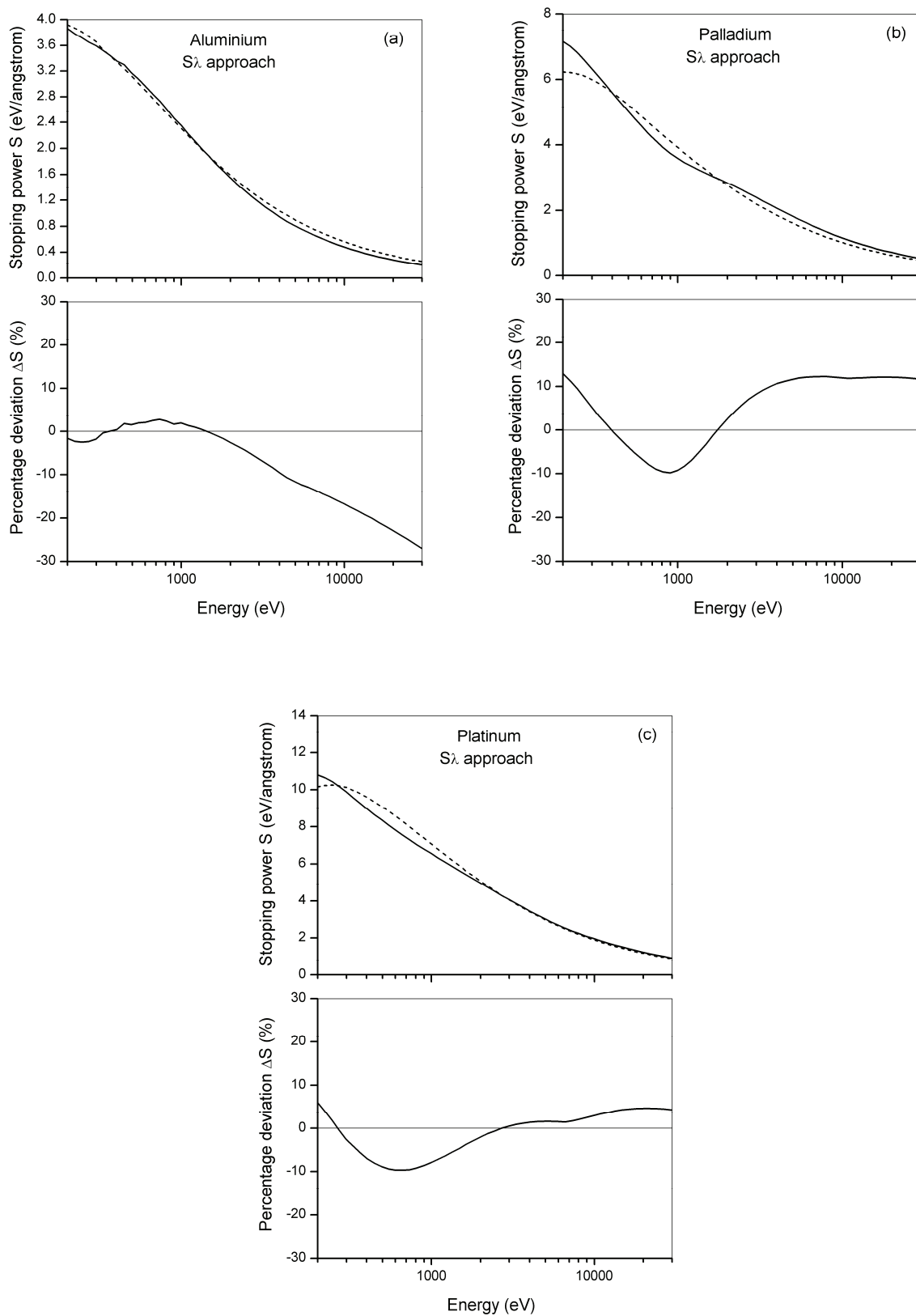
Fig. 2. Upper panels: Comparison of SPs obtained from optical data (solid lines) with SPs calculated from the predictive formula [Eq. (11)] (dashed lines) as a function of electron energy. Lower panels: The percentage difference, ΔS, between SPs from the two sources calculated from Eq. (12). (a) aluminum; (b) palladium; (c) platinum.

Journal of Surface Analysis Vol.15, No. 2 (2008) pp. 139−149

A. Jablonski et al.   Effects of Electron Backscattering in Auger Electron Spectroscopy: Recent Developments
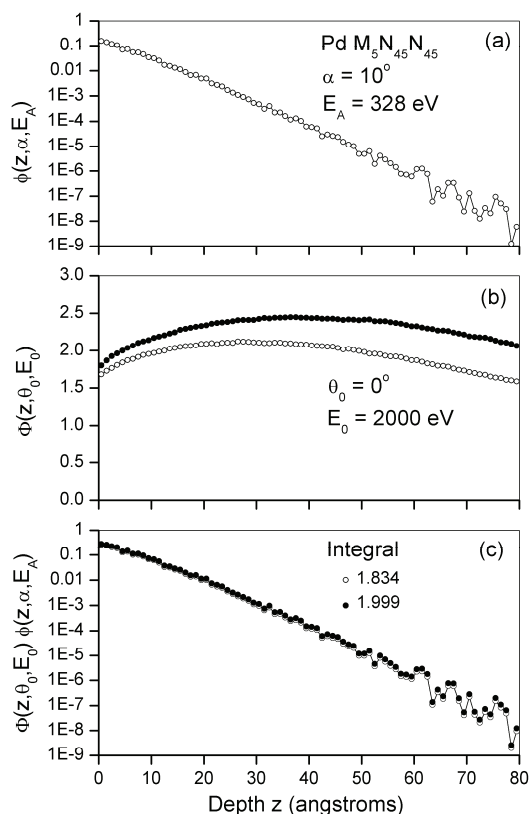
Fig. 3. Exemplary calculations of the BF for the Pd $M_5N_{45}N_{45}$ Auger transition from the general formula [Eq. (7)]. (a) The EMDDF calculated for an emission angle α = 10°; (b) the EXDDF calculated for a primary energy of 2 000 eV and for normal incidence; (c) product of the EMDDF and the EXDDF. Open circles: algorithm simulating separate inelastic interactions; solid circles: algorithm implementing the CSDA and the stopping power to describe inelastic scattering. In (b) and (c), the open circles show results from the EXDDF algorithm simulating separate inelastic interactions and the solid circles show results from the EXDDF algorithm implementing the CSDA and the stopping power to describe inelastic scattering.

obtain the BF. The BF from the most realistic algorithm (involving simulation of separate inelastic-scattering events) was 1.834 in this example whereas the corresponding BF from the approximate algorithm (CSDA and use of the SP to describe inelastic scattering) was 1.999. The BF from the approximate algorithm was thus 9 % larger than the BF from the realistic algorithm.

The BF calculations were made for normal incidence of the primary beam and with primary energies from slightly above E_c for each solid to 20 keV. The BF is, in general, a function of the emission angle, α [Eq. (7)], and previous work has shown a weak dependence of r on α

[9-12]. To determine the maximum range of variation of the BF with α, calculations were made for an emission angle close to normal (α=10°) and for a grazing emission angle (α=80°).

The BF results are shown in Figs. 4(a)-(c). For all three solids, BFs calculated from algorithm A generally differed from BFs obtained with algorithm B. In order to quantify the differences in BFs from the two algorithms, the following percentage deviation was calculated,

$$\Delta r = 100 \frac{r_A - r_B}{r_A}, \qquad (13)$$

where r_A is the reference BF from algorithm A and r_B is the BF obtained from algorithm B. The dependence of Δr on primary energy, in the range of interest for practical AES (> 3 keV), is shown in Fig. 5. For the worst case (Al $KL_{23}L_{23}$ in Fig. 5(a)), we see that Δr increases with energy from 4.2 % to 9.4 %. This increasing error can be correlated with the increasing difference, from -6.3 % to -27 % for the same energy range, between SPs from Eq. (11) and optical data shown in Fig. 2(a). For the Pd $M_5N_{45}N_{45}$ Auger transition (Fig. 5(b)), Δr decreases from 8.6 % at 3 keV to 2.5 % at 20 keV. Over this energy range, there is a nearly constant 10 % difference of the predicted SPs from the optical values, as shown in Fig 2(b). Finally, Δr for the Pt $M_5N_{67}N_{67}$ Auger transition (Fig. 5(c)) decreases with energy from 7.4 % at 3 keV to 1.3 % at 20 keV, although Δr varies between only 1 % and 2 % over most of the energy range, i.e., above 5 keV. Over the 3 keV to 20 keV range, the difference between predicted and optical SPs generally increases from 0.5 % to 4.6 %. It is clear that larger deviations between predicted and optical SPs lead to larger differences in BFs from algorithms A and B, and that a more reliable SP predictive formula is needed to obtain more accurate BFs from algorithm B.

Differences between BFs from algorithms A and B can also arise from use of the CSDA approximation, i.e., the neglect of straggling (the statistical spread of energies following inelastic scattering). Comparisons have been made of BFs calculated using algorithm A and a given energy-loss function with BFs obtained with algorithm B and SPs derived from the same energy-loss function. Jablonski *et al.* [24] found BF differences from these two approaches for the copper M_3VV, silver M_5VV and gold $N_{67}VV$ Auger transitions were negligibly small (< 1 %)

Journal of Surface Analysis Vol.15, No. 2 (2008) pp. 139−149

A. Jablonski et al.   Effects of Electron Backscattering in Auger Electron Spectroscopy: Recent Developments

for primary energies exceeding 1 keV. At lower energies, deviations of up to 10 % were found (due to a numerical approximation); such low primary energies, however, are not used in practical AES.

Figure 5 also shows that Δr is practically independent of the emission angle, α. We can conclude that the dependence of the BF on emission angle from algorithms A and B differ by an approximately constant factor. This expectation is confirmed in Fig. 6 which shows that the BF dependence on α from the two algorithms for the Pt $M_5N_{67}N_{67}$ transition are close to parallel for selected energies between 2936 eV and 20 keV. The shapes of the dependences, however, vary with primary energy. At 2936 eV, the BF increases with emission angle while it decreases for the higher energies shown.

The energy dependences of the BFs presented in Fig. 4 confirm previous results showing that r is a function of α,

but this dependence is not pronounced [9,10,12]. We see also that BFs from the general definition [Eq. (7)] can become smaller than unity, a result that would not be expected from the previous definition [Eq. (2)]. This result is due mainly to reduction of the primary-beam energy due to inelastic scattering in the near-surface region of the sample and the rapid variation of the inner-shell ionization cross section with energy for energies close to the ionization threshold. Such low energies are not typically used in practical AES although the BF could be less than unity for higher primary energies when the beam is at near-grazing angles of incidence.

Figure 4 also shows a comparison of BFs from the Shimizu equation for $\theta_0=0°$ [Eq. 6(a)] and primary energies between 3 keV and 10 keV (the range of the Shimizu and Ichimura calculations [5-7]) with our calculated BFs. The Shimizu equation does not, of course,
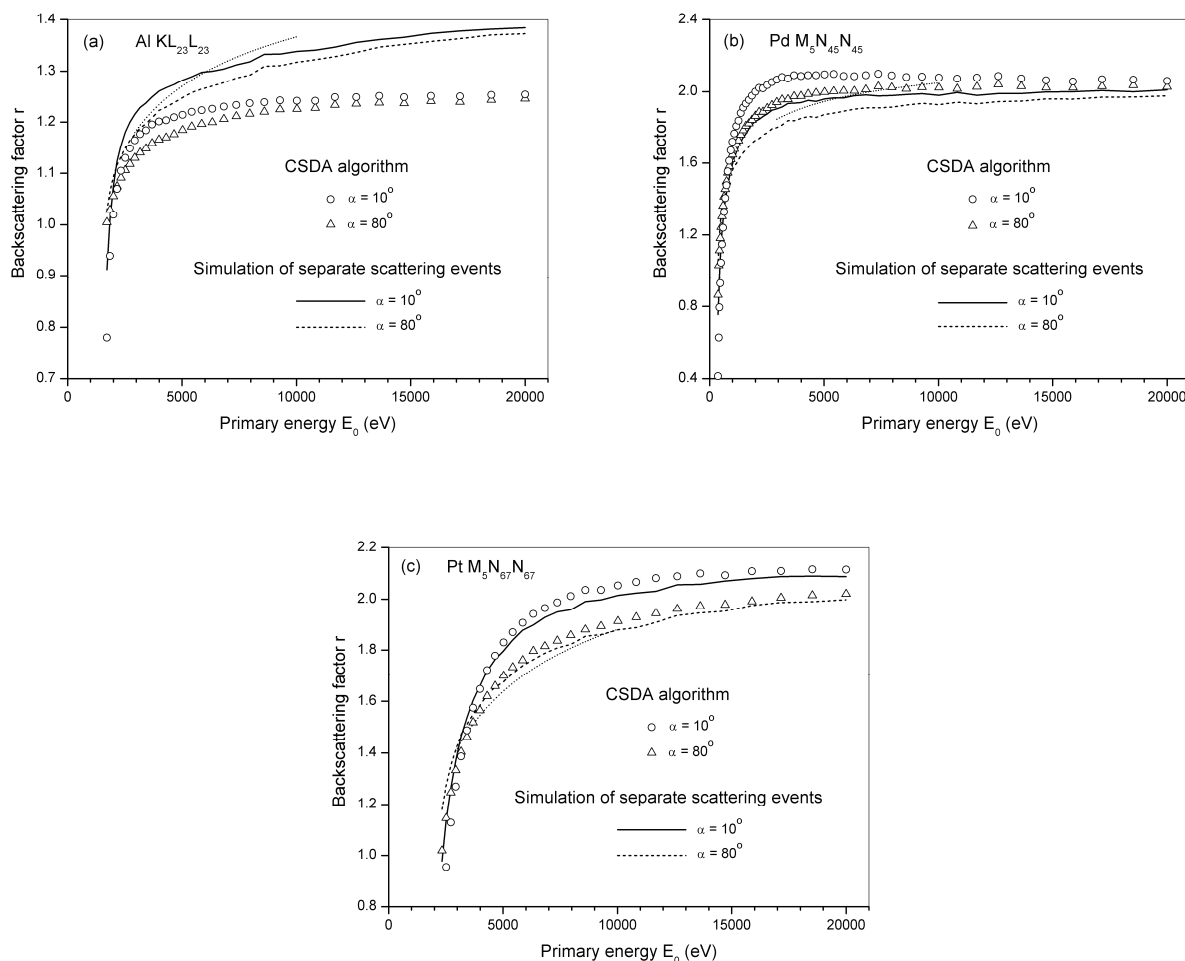

Fig. 4. Dependence of the BF on the primary-electron energy. Solid and dashed lines: algorithm A for the indicated emission angles; dotted line: Shimizu formula [Eq. (6a)]; symbols: algorithm B for the indicated emission angles. (a) Al $KL_{23}L_{23}$ Auger transition; (b) Pd $M_5N_{45}N_{45}$ Auger transition; (c) Pt $M_5N_{67}N_{67}$ Auger transition.

Journal of Surface Analysis Vol.15, No. 2 (2008) pp. 139−149

A. Jablonski et al.   Effects of Electron Backscattering in Auger Electron Spectroscopy: Recent Developments

show any dependence on α. The BFs from the Shimizu equation should most usefully be compared with BFs from algorithm A, the lines in Fig. 4 for $\alpha=0°$ and $\alpha=80°$. Our calculated BFs for the Al $KL_{23}L_{23}$ transition in Fig. 4(a) show a weaker dependence on E_0 than found from Eq. 6(a). The energy dependences of the BFs for the Pd $M_5N_{45}N_{45}$ and Pt $M_5N_{67}N_{67}$ transitions from Eq. 6(a) are closer to those found in our calculations [Figs. 4(b) and (c)]. For the three metals, the magnitudes of the BF from Eq. 6(a) are generally close to our values for either $\alpha=10°$ or $\alpha=80°$.
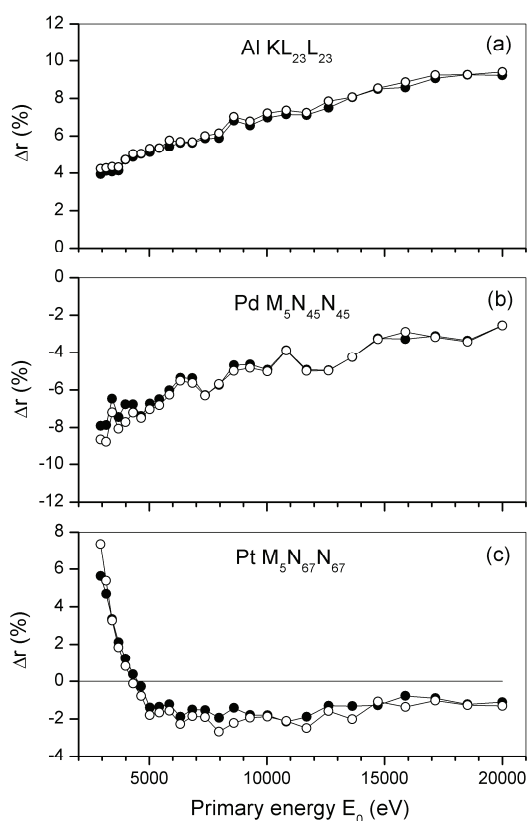
solid: the differential elastic-scattering cross sections for all atomic species constituting the solid, and the stopping power. It would be very difficult, if ever possible, to propose a simple and reliable analytical function of these variables that could be used to approximate BFs from Monte Carlo calculations. It seems that the best source of BFs in the future would be a computer-controlled data-base containing BFs from extensive Monte Carlo simula-tions. In fact, such a database is planned to be developed in the near future.

Fig. 5. The percentage differences, Δr, between BFs calculated from algorithms A and B [Eq. (13)]. Open circles: $\alpha=10°$; solid circles: $\alpha=80°$. (a) Al $KL_{23}L_{23}$ Auger transition; (b) Pd $M_5N_{45}N_{45}$ Auger transition; (c) Pt $M_5N_{67}N_{67}$ Auger transition.
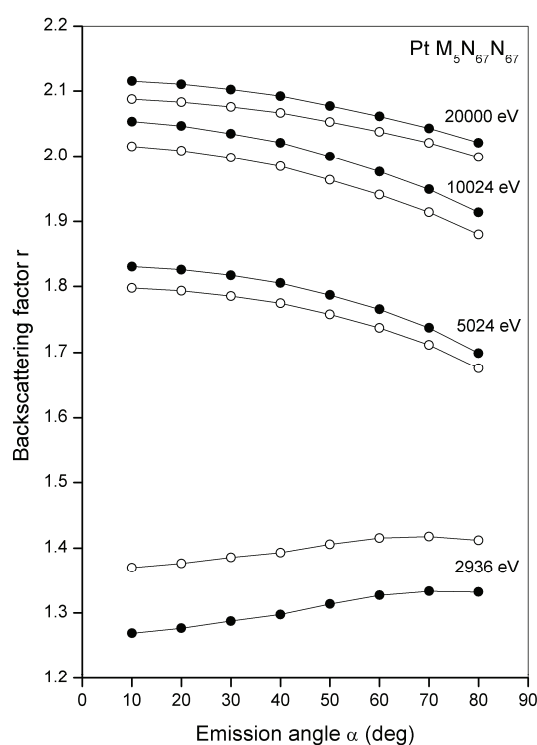

Fig. 6. Emission-angle dependence of the BF for the Pt $M_5N_{67}N_{67}$ Auger transition for primary-electron energies of 2 936 eV, 5024 eV, 10024 eV, and 20000 eV. Open circles: algo-rithm A; solid circles: algorithm B.

5. Conclusions

Equation (7) indicates that the BF is a function of five parameters: the inner-shell ionization-threshold energy, E_c, the Auger electron energy, E_A, the primary energy, E_0, the primary-beam incidence angle, θ_0, and the Au-ger-electron emission angle, α. In addition, the BF de-pends on the electron-transport characteristics of a given

We have presented calculations of BFs for three se-lected Auger transitions (Al $KL_{23}L_{23}$, Pd $M_5N_{45}N_{45}$, and Pt $M_5N_{67}N_{67}$) in the corresponding elemental solids using two algorithms. With algorithm A, BF values were ob-tained from Eq. (7) with a Monte Carlo calculation of the EXDDF in which individual inelastic-scattering events were simulated [10]. With the more approximate algo-rithm B, BFs were calculated using Eq. (7) and the

Journal of Surface Analysis Vol.15, No. 2 (2008) pp. 139−149

A. Jablonski et al.   Effects of Electron Backscattering in Auger Electron Spectroscopy: Recent Developments

EXDDF was found using the CSDA with predicted SPs from Eq. (11).

For primary-beam energies between 3 keV and 20 keV, differences in BFs from the two algorithms ranged from 4 % to 9 % for the Al $KL_{23}L_{23}$ transition, 2.5 % to 8 % for the Pd $M_5N_{45}N_{45}$, and 1.3 % to 7 % for the Pt $M_5N_{67}N_{67}$ transition. These differences arise mainly from use of an approximate predictive formula for the stopping power with algorithm B. Nevertheless, the differences are believed to be sufficiently small to enable use of the faster and more generally applicable algorithm B for calculating BFs in a wide range of solids and for a wide range of measurement conditions.

The calculated BFs show a weak dependence on Auger-electron emission angle, α. The BF dependences on α from algorithms A and B differed by an approximately constant factor although the shapes of the dependences varied with primary energy.

The effects of backscattered electrons need to be considered in other AES applications, e.g., the determination of composition profiles with depth by AES [35] and in determinations of the lateral resolution and information radius in high-spatial-resolution scanning Auger electron microscopy [36]. The use of the faster and more general algorithm B in future investigations should expedite progress in these other areas.

6. Acknowledgment

7. References

[1] H. E. Bishop and J. C. Riviere, *J. Appl. Phys.* **40**, 1740 (1969).

[2] K. Goto, K. Ishikawa, T. Koshikawa, and R. Shimizu, *Appl. Phys. Lett.* **24**, 358 (1974).

[3] K. Goto, K. Ishikawa, T. Koshikawa, and R. Shimizu, *Surf. Sci.* **47**, 477 (1975).

[4] A. Jablonski, *Surf. Interface Anal.* **1**, 122 (1979).

[5] R. Shimizu and S. Ichimura, *Quantitative Analysis by Auger Electron Spectroscopy*, Toyota Foundation Research Report No. I-006 76-0175, Tokyo, 1981.

[6] S. Ichimura and R. Shimizu, *Surf. Sci.* **112**, 386 (1981).

[7] S. Ichimura, R. Shimizu, and J. P. Langeron, *Surf. Sci.* **124**, L49 (1983).

[8] R. Shimizu, *Jpn. J. Appl. Phys.* **22**, 1631 (1983).

[9] A. Jablonski, *Surf. Sci.* **499**, 219 (2002).

[10] A. Jablonski and C. J. Powell, *Surf. Sci.* **574**, 219 (2005).

[11] Z. J. Ding, W. S. Tan, and Y. G. Li, *J. Appl. Phys.* **99**, 084903 (2006).

[12] A. Jablonski and C. J. Powell, *Surf. Sci.* **601**, 965 (2007).

[13] *Annual Book of ASTM Standards 2006*, Vol. 03.06, Standard Terminology Relating to Surface Analysis, Standard E 673-03, ASTM International, West Conshohocken, Pennsylvania (2006), p. 647.

[14] ISO Standard 18115: *Surface Chemical Analysis – Vocabulary*, International Organization for Standardization, Geneva, 2001.

[15] A. Jablonski and C. J. Powell, *J. Vac. Sci. Technol. A* **21**, 274 (2003).

[16] I. S. Tilinin and W. S. M. Werner, *Phys. Rev. B* **46**, 13739 (1992).

[17] I. S. Tilinin, A. Jablonski, J. Zemek, and S. Hucek, *J. Electron Spectrosc. Relat. Phenom.* **87**, 127 (1997).

[18] V. I. Nefedov and I. S. Fedorova, *J. Electron Spectrosc. Relat. Phenom.* **85**, 221 (1997).

[19] V. I. Nefedov, *J. Electron Spectrosc. Relat. Phenom.* **100**, 1 (1999).

[20] A. Jablonski, Surf. Science **586**, 115 (2005).

[21] S. Tougaard, *Solid State Commun.* **61**, 547 (1987).

[22] A. Jablonski and S. Tougaard, *Surf. Interface Anal.* **25**, 688 (1997).

[23] S. Tougaard, *Surf. Interface Anal.* **25**, 137 (1997).

[24] A. Jablonski, C. J. Powell, and S. Tanuma, *Surf. Interface Anal.* **37**, 861 (2005).

[25] S. Tanuma, C. J. Powell, and D. R. Penn, *Surf. Interface Anal.* **37**, 978 (2005).

[26] S. Tanuma, C. J. Powell, and D. R. Penn (to be published).

[27] A. Jablonski, S. Tanuma, and C. J. Powell, *Surf. Interface Anal.* **38**, 76 (2006).

[28] A. Jablonski, S. Tanuma, and C. J. Powell, *J. Surface Anal.* **13**, 170 (2006).

[29] A. Jablonski, F. Salvat, and C. J. Powell, *NIST Electron Elastic-Scattering Cross-Section Database*, Version 3.1, Standard Reference Data Program Database 64, U.S. Department of Commerce, National Institute of Standards and Technology, Gaithersburg,

Journal of Surface Analysis Vol.15, No. 2 (2008) pp. 139−149

A. Jablonski et al.   Effects of Electron Backscattering in Auger Electron Spectroscopy: Recent Developments

MD, 2003; web address: http://www.nist.gov/srd/nist64.htm.

[30] E. Casnati, A. Tartari, and C. Baraldi, *J. Phys. B* **15**, 155 (1982).

[31] M. P. Seah and I. S. Gilmore, *Surf. Interface Anal.* **26**, 815 (1998).

[32] C. D. Wagner, A. V. Naumkin, A. Kraut-Vass, J. W. Allison, C. J. Powell and J. R. Rumble Jr., *NIST X-ray Photoelectron Spectroscopy Database*, Version 3.4 (Web Version), Standard Reference Data Program Database 20, National Institute of Standards and Technology, Gaithersburg, 2003; web address: http://srdata.nist.gov/xps/).

[33] S. Tanuma, C. J. Powell, and D. R. Penn, Surf. Interface Anal. **17** (1991) 911.

[34] C. J. Powell and A. Jablonski, *NIST Electron Inelastic-Mean-Free-Path Database*, Version 1.1, Standard Reference Data Program, Database 71, National Institute of Standards and Technology, Gaithersburg, 2000.

[35] S. Hofmann, J. Y. Wang, and A. Zalar, *Surf. Interface Anal.* **39**, 787 (2007).

[36] A. Jablonski and C. J. Powell, *Appl. Surf. Sci.* **242**, 220 (2005).